Flight-Test Evaluation of Sensor Fusion Algorithms for Attitude Estimation

JASON N. GROSS, Student Member, IEEE
YU GU, Member, IEEE
MATTHEW B. RHUDY
SRIKANTH GURURAJAN
MARCELLO R. NAPOLITANO
West Virginia University

In this paper, several Global Positioning System/inertial navigation system (GPS/INS) algorithms are presented using both extended Kalman filter (EKF) and unscented Kalman filter (UKF), and evaluated with respect to performance and complexity. The contributions of this study are that attitude estimates are compared with independent measurements provided by a mechanical vertical gyroscope using 23 diverse sets of flight data, and that a fundamental difference between EKF and UKF with respect to linearization is evaluated.

Manuscript received January 16, 2011; revised May 16, 2011; released for publication July 5, 2011.

IEEE Log No. T-AES/48/3/944006.

Refereeing of this contribution was handled by M. Braasch.

This work was supported in part by the West Virginia Department of Highway under Project RP253-B.

Authors' address: Department of Mechanical and Aerospace Engineering, West Virginia University, 357 Engineering Sciences Bldg., 395 Evansdale Dr., Morgantown, WV 26506, E-mail: (Jason.N.Gross@gmail.com).

NOMENCLATURE

A	State transition matrix
a	Acceleration in the body-axis frame (m/s^2)
b	Bias
b_c	Body-axis coordinate frame
c	Statistical weighted linear regression bias
$\mathbf{d}$	Observation function input vector
e	Statistical weighted linear regression error
f	State transition function
g	Acceleration due to gravity (m/s^2)
H	Observation matrix
h	Observation function
i	Sigma-point index
J	Performance cost function
K	Kalman gain matrix
k	Discrete time index
L	Dimension of augmented state vector during prediction
l_c	Local geodetic coordinate frame
M	Dimension of augmented state vector during measurement update
n	Measurement noise
P	Error covariance matrix
p	Roll rate (deg/s)
Q	Process noise covariance matrix
q	Pitch rate (deg/s)
R	Measurement noise covariance matrix
r	Yaw rate (deg/s)
$\mathbf{u}$	State transition function input vector
V_x, V_y, V_z	Velocity in the local geodetic navigation frame (m/s)
w	Weight vector
$\mathbf{x}$	State vector
x, y, z	Position in the local geodetic navigation frame (m)
Y	Output sigma points
$\mathbf{y}$	Output vector
$\mathbf{z}$	Measurement vector
θ	Pitch angle (deg)
λ	Sigma-point scaling parameter
ν	Process noise
σ	Standard deviation
v	Random walk variance
ϕ	Roll angle (deg)
χ	Sigma points
ψ	Yaw angle (deg).

I. INTRODUCTION

The use of unmanned aerial vehicles (UAVs) for civil applications has substantially increased in recent years following the advancements of sensors and microprocessors [1–5]. Within these applications, accurate knowledge of attitude information is often required [1, 4]; on the other hand, the overall system weight and cost must be minimized [2, 5]. The conflict between these two requirements prevents

the use of high quality inertial navigation systems (INSs) typically used on military UAVs [3, 5]. Additionally, many applications have real-time processing requirements [6], while others depend on accurate postprocessing [7]. Therefore, there is a clear need for developing algorithms that rely on low-cost components and are evaluated with respect to both accuracy and computational requirements.

For UAV-based remote sensing applications, such as 3-D mapping with direct geo-referencing [8] or constructing large image mosaics [7], high fidelity aircraft attitude information is a key requirement. In addition, in the application of airborne visual target tracking, it was recently noted that tracking error is most sensitive to attitude uncertainty [6]. Recent advances of micro-electro-mechanical systems (MEMS) technology have made low-cost inertial measurement units (IMUs) available; however, the limited accuracy of these components does not make them adequate alone due to the accumulation of the sensor biases over time [9]. The high accuracy of Global Positioning System (GPS) velocity measurements has also lead researchers to develop single GPS antenna-based attitude solutions. For example, Kornfeld, Hansman, and Deyst [10, 11] estimated aircraft pseudo-attitude based on only GPS velocity measurements [10], and showed its effectiveness toward detecting inertial sensor failures [11]. The functional integration of a low-cost INS and a GPS receiver has well-known benefits [12, 13]. The most notable advantage is that the unbiased solution offered by a GPS receiver regulates the low frequency drift associated with low-cost inertial systems, and the high frequency errors present in the GPS measurements are smoothed by inertial measurements [14]. Several GPS/INS formulations have been developed that vary in terms of the number of navigation states estimated [14, 15] and the form of GPS information used for measurement update [16]. This paper focuses on investigating attitude estimation solutions that rely on a loosely-coupled [12] integration of low-cost GPS/INS sensors, in terms of both accuracy and computational efficiency.

The nonlinearities associated with inertial navigation equations often require the use of a nonlinear estimator [15, 17, 18] in a GPS/INS sensor fusion algorithm, to combine the information in a predictor-corrector framework. Two popular nonlinear estimators, the extended Kalman filter (EKF) [19] and the unscented Kalman filter (UKF) [20], have been applied to this problem [15–18], however, there are still questions regarding their benefits and drawbacks. Specifically, van der Merwe and Wan [17] report superior estimation performance of UKF over EKF in handling the nonlinearities present in a GPS/INS application, while Crassidis reports that UKF outperforms EKF for GPS/INS when dealing with large initialization errors [15]. Wendel, et al. state that significant performance increase of UKF over EKF is found only when confronted with large initialization errors, and essentially no difference otherwise [16] in a tightly-coupled GPS/INS sensor fusion application. Additionally, with respect to computational requirements, van der Merwe, et al. note that the computation complexity order of the algorithms are the same [17], while St. Pierre and Ing [21] contend, with empirical results, that the UKF is computationally more expensive than EKF. Furthermore, it has been stated that a problem associated with EKF implementation is that it is difficult to "tune" in comparison to the UKF framework [20].

The above conflicting conclusions demonstrate that many issues have yet to be fully addressed. Toward improving the level of knowledge in this field, this effort focuses on evaluating performances of multiple GPS/INS sensor fusion algorithms using UAV flight data with independent attitude "truth" measurements. Specifically, instead of using simulated data for performance analysis as in earlier comparison studies [15–17], a total of 23 sets of flight data were selected, from more than 150 data sets collected over seven years using West Virginia University's (WVU) three jet-powered YF-22 UAVs [22], to represent diversity in terms of operation temperature, wind conditions, mission profile, and sensor payload configurations. In each of these flights, a mechanical vertical gyroscope is used to provide an independent measurement of aircraft pitch and roll angles. These measurements are used as truth data for comparison with aircraft attitude angles estimated using different GPS/INS sensor fusion algorithms. The goal of using several sensor fusion formulations with a diverse set of flight data is to gain deeper insights into the relative advantages and disadvantages of applying either EKF or UKF to GPS/INS based attitude estimation.

The rest of the paper is organized as follows. Section II describes several GPS/INS sensor fusion algorithms as well as some fundamental differences between EKF and UKF implementations. Section III discusses the experimental UAV sensor systems and selected flight data. Section IV presents results both with respect to the computational load and estimation performance; finally, Section V provides the conclusion of this study.

II. SENSOR FUSION ALGORITHMS

Most GPS/INS sensor fusion algorithms combine two information sources for attitude estimation: the time integration of rate gyroscopes and the known direction of the Earth's gravitational vector. In a static setting, by referencing the Cartesian components of Earth's gravitational vector, 3-axis accelerometers can be used as a tilt sensor to determine attitude [23]. In a dynamic environment, however, accelerometers alone

cannot distinguish between inertial and gravitational accelerations. In these situations, a GPS receiver can be used to provide information to isolate the two acceleration components, and in this sense, the GPS/accelerometers combination acts as a dynamic tilt sensor.

Within this paper, several GPS/INS algorithms are investigated. For each algorithm, Euler rotation angles are estimated to provide a simple and intuitive mathematical representation of aircraft attitude. This was chosen over the singularity-free quaternion-based attitude representation in order to avoid additional algorithm complexities associated ensuring quaternion unity norm requirement [24], and Euler angle singularity points are rarely encountered within many aerial UAV applications, and can be monitored on-line [25].

A. Acceleration Vector Attitude Estimation (AVAE)

An acceleration vector attitude estimation (AVAE) algorithm is developed for direct attitude estimation following the dynamic tilt sensor concept. The AVAE algorithm features GPS acceleration in a local geodetic frame (l_c), estimated by numerical differentiation of GPS velocity measurements, and accelerometer measurements obtained in the aircraft body-axis (b_c). The aircraft Euler angles, roll (ϕ), pitch (θ), and yaw (ψ), define a direction cosine matrix (DCM) between the two coordinate frames [26]

$$\begin{bmatrix} a_x \\ a_y \\ a_z \end{bmatrix}_{(b\_c)} = \begin{bmatrix} 1 & 0 & 0 \\ 0 & \mathrm{c}\phi & \mathrm{s}\phi \\ 0 & -\mathrm{s}\phi & \mathrm{c}\phi \end{bmatrix} \begin{bmatrix} \mathrm{c}\theta & 0 & -\mathrm{s}\theta \\ 0 & 1 & 0 \\ \mathrm{s}\theta & 0 & \mathrm{c}\theta \end{bmatrix} \times \begin{bmatrix} \mathrm{c}\psi & \mathrm{s}\psi & 0 \\ -\mathrm{s}\psi & \mathrm{c}\psi & 0 \\ 0 & 0 & 1 \end{bmatrix} \begin{bmatrix} a_x \\ a_y \\ a_z - g \end{bmatrix}_{(l\_c)} \tag{1}$$

where a is acceleration and g is the acceleration due to gravity. With measurements from both GPS and accelerometers, the projection of the local gravity vector on the three aircraft body-axes in terms of the three Euler angles can then be solved, as demonstrated by Kingston, et al. [14].

To reduce the matrix relationship shown in (1), yaw angle (ψ) is approximated with the aircraft heading angle (Ψ) which is directly obtained by calculating the instantaneous four-quadrant inverse tangent (e.g. atan 2) to the aircraft trajectory using GPS velocity measurements in the x and y axes within the (l_c) coordinate frame:

$$\psi \approx \Psi = \tan^{-1}\left(\frac{V_{y(l\_c)}}{V_{x(l\_c)}}\right). \tag{2}$$

The two remaining aircraft Euler angles are then estimated by considering sequential Euler rotations. Specifically, by considering the rotation through the heading angle, an intermediate acceleration vector, denoted with subscript (ψ), is defined as

$$\begin{bmatrix} a_x \\ a_y \\ a_z \end{bmatrix}_{(\psi)} = \begin{bmatrix} a_{x(l\_c)}\cos\psi + a_{y(l\_c)}\sin\psi \\ a_{y(l\_c)}\cos\psi - a_{x(l\_c)}\sin\psi \\ a_{z(l\_c)} - g \end{bmatrix} \tag{3}$$

which leads to the following algebraic equations:

$$\begin{bmatrix} a_x \\ a_y \\ a_z \end{bmatrix}_{(b\_c)} = \begin{bmatrix} \cos\theta & 0 & -\sin\theta \\ \sin\phi\sin\theta & \cos\phi & \sin\phi\cos\theta \\ \cos\phi\sin\theta & -\sin\phi & \cos\phi\cos\theta \end{bmatrix} \times \begin{bmatrix} a_x \\ a_y \\ a_z \end{bmatrix}_{(\psi)}. \tag{4}$$

The first equation of the above set can be solved for the pitch angle,

$$\theta = \tan^{-1}\left(\frac{a_{x(\psi)}a_{z(\psi)} + a_{x(b\_c)}\sqrt{a_{x(\psi)}^2 + a_{z(\psi)}^2 - a_{x(b\_c)}^2}}{a_{z(\psi)}^2 - a_{x(b\_c)}^2}\right). \tag{5}$$

By again rotating the $a_{(\psi)}$ acceleration vector with the newly obtained pitch estimate, a second intermediate acceleration vector, denoted with subscript (ψ,θ), leaves the roll angle as the only unknown variable,

$$\begin{bmatrix} a_x \\ a_y \\ a_z \end{bmatrix}_{(b\_c)} = \begin{bmatrix} 1 & 0 & 0 \\ 0 & \cos\phi & \sin\phi \\ 0 & -\sin\phi & \cos\phi \end{bmatrix} \begin{bmatrix} a_x \\ a_y \\ a_z \end{bmatrix}_{(\psi,\theta)} \tag{6}$$

which can be algebraically solved using

$$\phi = \tan^{-1}\left(\frac{-a_{y(\psi,\theta)}a_{z(\psi,\theta)} - a_{y(b\_c)}\sqrt{a_{y(\psi,\theta)}^2 + a_{z(\psi,\theta)}^2 - a_{y(b\_c)}^2}}{a_{z(\psi,\theta)}^2 - a_{y(b\_c)}^2}\right). \tag{7}$$

Within the AVAE algorithm, the GPS acceleration vector is calculated using a numerical backward-difference derivative of the GPS velocity measurement vector. To reduce the noise associated with the numerical derivative, the pitch and roll estimates obtained with the AVAE formulation are smoothed with a first-order low-pass Butterworth filter.

B. 3-State Sensor Fusion Formulation

While the AVAE algorithm provides estimates of all three aircraft Euler angles, it does not take advantage of information provided by low-cost rate gyroscopes, which are readily available in MEMS IMUs. In this context, a 3-state GPS/INS sensor fusion algorithm is formulated as a state estimation problem in a traditional predictor-corrector framework

with a Kalman filter (KF). Within this framework, five major components are defined: a state vector $\mathbf{x}$, an input vector $\mathbf{u}$, a set of nonlinear state transition functions f, a set of nonlinear observation functions h, and a measurement vector $\mathbf{z}$.

In the 3-state formulation, the aircraft Euler angles, denoted as $\mathbf{x} = [\phi \ \theta \ \psi]^T$, are first predicted using the roll rate p, pitch rate q, and yaw rate r, measured in the aircraft body-axis (b_c) and denoted by $\mathbf{u} = [p \ q \ r]^T_{(b\_c)}$ using the relationships [27]:

$$\dot{\phi} = (p + q\sin\phi\tan\theta + r\cos\phi\tan\theta) + \nu_\phi \tag{8}$$

$$\dot{\theta} = (q\cos\phi - r\sin\phi) + \nu_\theta \tag{9}$$

$$\dot{\psi} = ((q\sin\phi + r\cos\phi)\sec\theta) + \nu_\psi \tag{10}$$

where (8)–(10) are the nonlinear state transition functions $f(\mathbf{x},\mathbf{u},v)$, and v represents process noise. Next, a measurement-update procedure is performed, which is conceptually equivalent to the AVAE algorithm. Within this procedure, the triad of IMU body-axis (b_c) specific-force measurements $\mathbf{d} = [a_x \ a_y \ a_z]^T_{(b\_c)}$ are transformed to the geodetic frame (l_c) using a DCM that defines the nonlinear observation function, $h(\mathbf{x},\mathbf{d},n)$, with the predicted attitude estimates provided by the rate gyros

$$\begin{bmatrix} \dot{V}_x \\ \dot{V}_y \\ \dot{V}_z + g \end{bmatrix}_{(l\_c)} = \begin{bmatrix} \mathrm{c}\psi\mathrm{c}\theta & -\mathrm{s}\psi\mathrm{c}\phi + \mathrm{c}\psi\mathrm{s}\theta\sin\phi & \mathrm{s}\psi\mathrm{s}\phi + \mathrm{c}\psi\mathrm{s}\theta\mathrm{c}\phi \\ \mathrm{s}\psi\mathrm{c}\theta & \mathrm{c}\psi\mathrm{c}\phi + \mathrm{s}\psi\mathrm{s}\theta\mathrm{s}\phi & -\mathrm{c}\psi\mathrm{s}\phi + \mathrm{s}\psi\mathrm{s}\theta\mathrm{c}\phi \\ -\mathrm{s}\theta & \mathrm{c}\theta\mathrm{s}\phi & \mathrm{c}\theta\mathrm{c}\phi \end{bmatrix} \begin{bmatrix} a_x \\ a_y \\ a_z \end{bmatrix}_{(b\_c)} + n \tag{11}$$

where n represents the measurement noise; the measurement vector $\mathbf{z}$ is acquired through differentiation of GPS velocity measurements.

C. 9-State Sensor Fusion Formulation

In the 3-state formulation, the DCM relating accelerometer measurements to GPS velocity is used for regulating attitude estimates obtained by integrating angular rate measurements from low-cost gyroscopes. This requires nonlinear functions to be present within both the state transition (8)–(10) and observation functions (11). If both rate gyro and accelerometer measurements are used for estimating aircraft attitude, velocity, and position in the prediction stage, then the measurement update is linear, using directly the GPS position and velocity measurements. This also removes the need for numerical differentiation of the GPS velocity as in AVAE and the 3-state formulation. Within this 9-state formulation, the navigation state vector ($\mathbf{x}$) considers a full position, velocity, and attitude (PVA) solution:

$$\mathbf{x} = [x_{l\_c} \quad y_{l\_c} \quad z_{l\_c} \quad V_{xl\_c} \quad V_{yl\_c} \quad V_{zl\_c} \quad \phi_{b\_c} \quad \theta_{b\_c} \quad \psi_{b\_c}]^T \tag{12}$$

where the position and velocity are in the local geodetic (l_c) frame, and the Euler angles are in the aircraft body axis (b_c). The continuous-time state transition equations f are given by

$$\dot{\mathbf{x}} = \begin{bmatrix} \dot{x} \\ \dot{y} \\ \dot{z} \\ \dot{V}_x \\ \dot{V}_y \\ \dot{V}_z \\ \dot{\phi} \\ \dot{\theta} \\ \dot{\psi} \end{bmatrix} = \begin{bmatrix} V_x \\ V_y \\ V_z \\ \mathrm{c}\psi\mathrm{c}\theta a_x + (-\mathrm{s}\psi\mathrm{c}\phi + \mathrm{c}\psi\mathrm{s}\theta\mathrm{s}\phi)a_y + (\mathrm{s}\psi\mathrm{s}\phi + \mathrm{c}\psi\mathrm{s}\theta\mathrm{c}\phi)a_z \\ \mathrm{s}\psi c\theta a_x + (\mathrm{c}\psi\mathrm{c}\phi + \mathrm{s}\psi\mathrm{s}\theta\mathrm{s}\phi)a_y + (-\mathrm{c}\psi\mathrm{s}\phi + \mathrm{s}\psi\mathrm{s}\theta\mathrm{c}\phi)a_z \\ -\mathrm{s}\theta a_x + \mathrm{c}\theta\mathrm{s}\phi a_y + \mathrm{c}\theta\mathrm{c}\phi a_z - g \\ p + q\mathrm{s}\phi\mathrm{t}\theta + r\mathrm{c}\phi\mathrm{t}\theta \\ q\mathrm{c}\phi - r\mathrm{s}\phi \\ (q\mathrm{s}\phi + r\mathrm{c}\phi)\sec\theta \end{bmatrix} + \nu. \tag{13}$$

In this sensor fusion formulation, the observation function is linear

$$H = [I_{6\times6} \quad 0_{6\times3}] \tag{14}$$

where the observation matrix simply extracts the predicted position and velocity states,

$$\mathbf{y} = H\mathbf{x} + n \tag{15}$$

to obtain an output vector, which is directly comparable with the GPS measured position and velocity: $\mathbf{z} = [x_{\mathrm{GPS}} \ y_{\mathrm{GPS}} \ z_{\mathrm{GPS}} \ V_{x_{\mathrm{GPS}}} \ V_{y_{\mathrm{GPS}}} \ V_{z_{\mathrm{GPS}}}]^T_{(l\_c)}$.

D. 15-State Sensor Fusion Formulation

Finally, a 15-state GPS/INS sensor fusion formulation is developed by augmenting the 9-state formulation with six time-varying bias states associated with the six IMU measurements. This approach has the added benefit of improving the performance of the prediction stage (12), but at the cost of added computational burden. The 15 estimated states include PVA states and six sensor biases and are given by

$$\mathbf{x} = [x_{l\_c} \quad y_{l\_c} \quad z_{l\_c} \quad V_{xl\_c} \quad V_{yl\_c} \quad V_{zl\_c} \quad \phi_{b\_c}\theta_{b\_c}\psi_{b\_c}b_{a_x} \quad b_{a_y} \quad b_{a_z} \quad b_p \quad b_q \quad b_r]^T \tag{16}$$

where b stands for sensor bias. During the state prediction procedure, the same relationships described in (12) account for the first nine state transition equations, with the exception that the bias states are subtracted from the raw IMU measurements

$$\mathbf{u} = [a_{xb\_c} - b_{a_x} \quad a_{yb\_c} - b_{a_y} \quad a_{zb\_c} - b_{a_z} \quad p_{b\_c} - b_p \quad q_{b\_c} - b_q \quad r_{b\_c} - b_r]^T. \tag{17}$$

In order to model the dynamics of the six bias states, the random walk (RW) assumption is used,

$$\dot{b} = v \tag{18}$$

which has been shown to apply to low-grade MEMS-based sensors [28]. The variance of the random noise v is determined based on each sensor's Allan variance as reported by the manufacturer.

The same measurement vector in the 9-state formulation is also used for the 15-state measurement update. The observation matrix is given by

$$H = [I_{6\times 6} \quad 0_{6\times 9}]. \tag{19}$$

E. Nonlinear Estimators: Extended Kalman Filter and Unscented Kalman Filter

The algorithms associated with the EKF and the UKF are well known and can be found in several publications [13, 19, 29, 17]. Two fundamental differences between EKF and UKF are summarized as a difference with respect to the method employed for linearization, and a difference in the way process and measurement noises are implemented within each algorithm. To facilitate this comparison, the EKF and UKF algorithms are first discussed; next, the distinctions between the two estimators are highlighted with respect to their implications for the GPS/INS sensor fusion formulations used in this study.

1) *Extended Kalman Filter*: For each GPS/INS sensor fusion formulation, the continuous state transition and observation functions are first discretized. For the EKF, the nonlinear state transition functions are used to predict the a priori state estimates $\hat{\mathbf{x}}_{k|k-1}$:

$$\hat{\mathbf{x}}_{k|k-1} = f(\mathbf{x}_{k-1|k-1}, \mathbf{u}_k) + \nu \tag{20}$$

where $\mathbf{u}_k$ is the input vector to the state transition function, and the additive process noise ν is assumed to be white, with a known covariance Q (i.e., $\nu \sim N(0,Q)$). A linearization of f is required to predict the a priori error covariance matrix $P_{k|k-1}$:

$$P_{k|k-1} = A_k P_{k-1|k-1} A_k^T + Q \tag{21}$$

where A_k is the Jacobian matrix of f with respect to $x_{k-1|k-1}$.

During the EKF measurement-update procedure, the estimated outputs $\mathbf{y}_k$ are directly comparable to the measurement vector $\mathbf{z}_k$. Using the nonlinear observation functions, $\mathbf{y}_k$ is calculated using

$$\mathbf{y}_k = h(\mathbf{x}_{k|k-1}, \mathbf{d}_k) + n \tag{22}$$

where $\mathbf{d}_k$ is the input vector to the observation functions, and n is the additive measurement noise, assumed to be white Gaussian, with $n \sim N(0,R)$. The Jacobian of the observation functions with respect to $\mathbf{x}_{k|k-1}$, H_k, is used to calculate the Kalman gain matrix,

$$K_k = P_{k|k-1} H_k^T (H_k P_{k|k-1} H_k^T + R)^{-1}. \tag{23}$$

K_k is then used to update the predicted states and error covariance:

$$\mathbf{x}_{k|k} = \mathbf{x}_{k|k-1} + K_k(\mathbf{z}_k - \mathbf{y}_k) \tag{24}$$

$$P_{k|k} = (I - K_k H_k) P_{k|k-1}. \tag{25}$$

2) *Unscented Kalman Filter*: UKF uses the unscented transformation to transform statistical information through nonlinear functions [20]. The UKF prediction stage starts with the augmentation of the state vector with the process noise $\mathbf{x}^a = [\mathbf{x}^T \ \ \nu^T]^T$. The mean and error covariance matrix for the augmented state vector is given as

$$\bar{\mathbf{x}}^a_{k-1|k-1} = [\mathbf{x}^T_{k-1|k-1} \quad 0]^T \qquad P^a_{k-1|k-1} = \begin{bmatrix} P_{k-1|k-1} & 0 \\ 0 & Q \end{bmatrix} \tag{26}$$

which are then used to generate a set of sigma points

$$\chi_{k-1|k-1} = \left[\bar{\mathbf{x}}^a_{k-1|k-1} \quad \bar{\mathbf{x}}^a_{k-1|k-1} + \lambda\sqrt{P^a_{k-1|k-1}} \quad \bar{\mathbf{x}}^a_{k-1|k-1} - \lambda\sqrt{P^a_{k-1|k-1}}\right] \tag{27}$$

where λ is a scaling parameter. Next, each of the sigma points is transformed through nonlinear state transition functions:

$$\chi^{i=0:2L}_{k|k-1} = f(\chi^{i=0:2L}_{k-1|k-1}, \mathbf{u}_k) \tag{28}$$

where L is the dimension of the augmented state vector. With the transformed sigma points, the predicted mean and error covariance are calculated

as weighted sums using

$$x_{k|k-1} = \sum_{i=0}^{2L} w_i^m \chi_{k|k-1}^i \tag{29}$$

$$P_{k|k-1} = \sum_{i=0}^{2L} w_i^C (\chi_{k|k-1}^i - x_{k|k-1})(\chi_{k|k-1}^i - x_{k|k-1})^T. \tag{30}$$

Details on assigning the weights and scaling parameters for a UKF can be found in [17].

During a UKF measurement-update, the state vector is augmented with the measurement noise $\mathbf{x}^a = [\mathbf{x}^T \ \ n^T]^T$, and the predicted mean from (29) and covariance from (30) are used to generate a new set of sigma points:

$$\bar{\mathbf{x}}_{k|k-1}^a = [\mathbf{x}_{k|k-1}^T \quad 0]^T, \qquad P_{k|k-1}^a = \begin{bmatrix} P_{k|k-1} & 0 \\ 0 & R \end{bmatrix} \tag{31}$$

$$\chi_{k|k-1} = \left[\bar{\mathbf{x}}_{k|k-1}^a \quad \bar{\mathbf{x}}_{k|k-1}^a + \lambda\sqrt{P_{k|k-1}} \quad \bar{\mathbf{x}}_{k|k-1}^a - \lambda\sqrt{P_{k|k-1}}\right] \tag{32}$$

which are then transformed through nonlinear observation functions:

$$Y_k^{i=0:2M} = h(\chi_{k|k-1}^i, \mathbf{d}_k) \tag{33}$$

where M is the dimension of the augmented state vector. Subsequently, the outputs, the observation error covariance, and the cross-covariance of the predicted states and observations are calculated as weighted sums of the transformed sigma points:

$$y_k = \sum_{i=0}^{2M} w_i^m Y_{k|k-1}^i \tag{34}$$

$$P_{\mathbf{yy}} = \left(\sum_{i=o}^{2M} w_i^C (Y_k^i - \mathbf{y}_k)(Y_k^i - \mathbf{y}_k)^T\right) \tag{35}$$

$$P_{\mathbf{xy}} = \left(\sum_{i=o}^{2M} w_i^C (\chi_{k|k-1}^i - \mathbf{x}_{k|k-1})(Y_k^i - \mathbf{y}_k)^T\right). \tag{36}$$

Finally, the UKF Kalman gain is calculated using

$$K_k = P_{\mathbf{xy}} P_{\mathbf{yy}}^{-1}. \tag{37}$$

The above gains are then used to update the predicted states and error covariance:

$$\mathbf{x}_{k|k} = \mathbf{x}_{k|k-1} + K_k(\mathbf{z}_k - \mathbf{y}_k) \tag{38}$$

$$P_{k|k} = P_{k|k-1} - K_k P_{\mathbf{yy}} K_k^T. \tag{39}$$

A clear difference between EKF and UKF is the use of analytical linearization by EKF as compared with the use of statistical linearization [30, 31] within UKF. Both 9-state and 15-state formulations presented above have nonlinear state transition functions and linear observation functions. Therefore, the EKF and UKF implementations are different only during the prediction step while the standard linear KF measurement update procedure [19, 29] is used for both filters. However, in the 3-state formulation, nonlinearity is present in both the prediction and update stages.

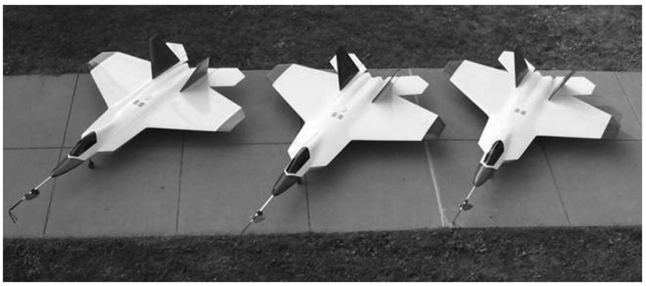

Fig. 1. YF-22 research UAV fleet.

Another major difference between EKF and UKF implementations presented is the method for handling the process and measurement noise. Specifically, within UKF, sigma points are generated according to known or assumed statistical distributions of sensor noise, which are then directly considered on the sensor outputs and transformed through nonlinear equations. This eliminates the need for additive process and measurement noise assumptions. Instead, EKF linearizes the nonlinear state transition and observation equations only with respect to states, and does not directly handle nonlinear relationships with respect to sensor noise. As a result, EKF implementation lumps different sources of noises as one set of additive noise, whose property is often difficult to determine in practical applications. For example, in the relationships (8)–(10) used in the prediction stage of all three sensor fusion formulations, the overall process noise is a nonlinear combination of rate gyroscope noises. In this case, if it is assumed that the noise of each individual rate gyroscope is white and Gaussian, the same assumption is not necessarily valid for the overall process noise. In general, it is possible to also derive a Jacobian that linearizes the state transition function about the assumed process noise within an EKF implementation [32], however the ability for UKF to easily handle noise at the sensor level though statistically linearization nonlinear relationships represents a practical implementation advantage over EKF.

III. EXPERIMENTAL SET-UP

This sensor fusion study was conducted using flight data collected on three WVU YF-22 research platforms. Each aircraft, shown in Fig. 1, is approximately 2.4 m long with a 2 m wing span, and a weight of approximately 22.5 Kg. The aircraft is powered with a miniature turbine that produces 125 N of static thrust.

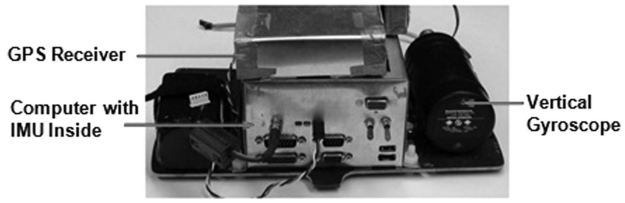

Fig. 2. YF-22 GPS/INS sensor fusion instrumentation.

The WVU YF-22 research platforms have been utilized for various research projects, including the validation of autonomous formation flight control laws [33], and fault-tolerant flight control laws [34]. Over the years, a large database of flight data was accumulated, which forms the foundation for this study. A typical flight test involves manually piloted and/or autonomous segments within a loitering loop pattern.

Flight data were collected with two different avionics architectures. Flights 1–21 were collected with avionic system 1 [22], with Crossbow V400A® IMUs and Novatel OEM4® GPS receivers. The Crossbow IMUs were sampled with a 16-bit resolution, over a full scale range of ±200°/s on the rate gyros, and ±10 g for the accelerometers. The OEM4 GPS receiver reports a 1.8 m circular error probable (CEP) for position measurements. Avionic system 2 [35] was used for Flights 22–23, on the blue YF-22 (triangle indicates blue YF-22* in Fig. 3). An Analog Devices ADIS-16405® IMU was used within system 2, which provides a 14-bit digital output for all acceleration and rate channels, with range of ±150°/s for the gyros, and ±18 g for the accelerometers. The GPS within system 2 was also a Novatel OEM4.

For both avionic systems, a Goodrich VG34® mechanical vertical gyroscope was used to provide independent pitch and roll angle measurements. The VG34 has a ±90° measurement range on the roll axis and a ±60° range on the pitch axis, and was sampled with 16-bit resolution. The VG34 has a self-erection system, and reported accuracy of within 0.25° of true vertical. The output of the mechanical vertical gyroscope was used as the truth data for the sensor fusion study. The avionic system 2 is shown in Fig. 2.

Within this study, 23 sets of flight data were considered, using three aircraft with four sets of on-board sensor payloads. These flights were selected from over 150 sets of flight data to represent a diverse range of temperature conditions, wind conditions, mission profile, and sensor platform. A distribution of selected flight data with respect to operating temperature and the research platform used is shown in the top half of Fig. 4, and the velocity distribution over the 23 flights are shown in the bottom half of Fig. 3. Within the top plot in Fig. 3, the flights numbers are ordered chronologically, and blue YF-22* represents the blue YF-22 aircraft with avionic system 2. The contour graph in Fig. 4 shows the distribution of all data samples with respect to pitch and roll angles, indicating dynamic flight conditions and a large flight envelope covered over the 23 flights.

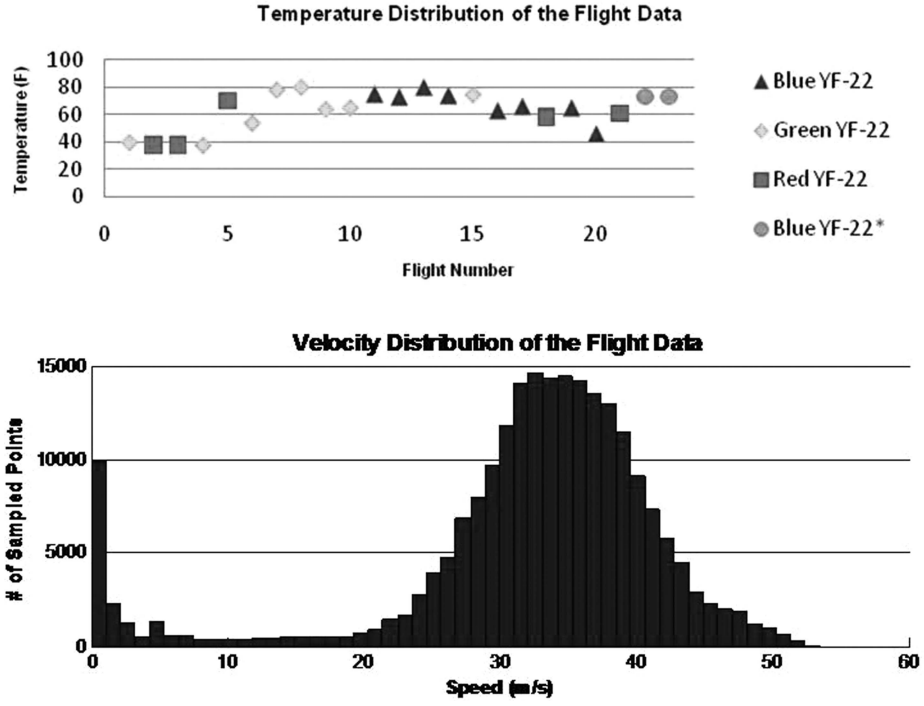

Fig. 3. Flight data vs. temperature (top) and velocity distribution (bottom).

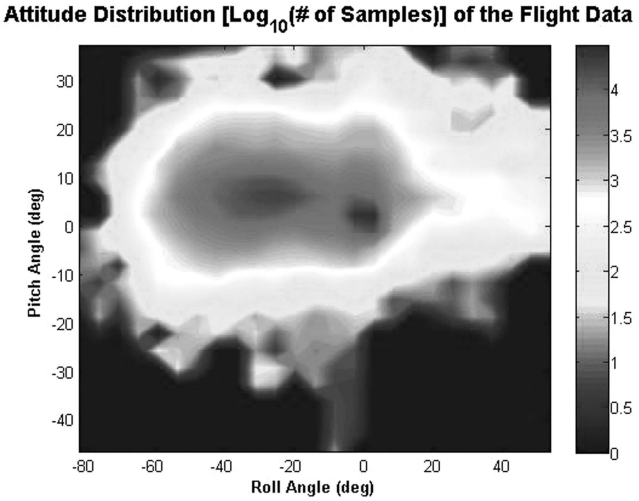

Fig. 4. Distribution of aircraft attitude samples over 23 flights.

IV. ATTITUDE ESTIMATION RESULT

A. Computational Load

For state estimation, Wan and van der Merwe point out that both EKF and UKF are $O(L^2)$ in terms of computational complexity, where L is the dimension of the state vector [36]. In order to empirically evaluate the computational requirements for each algorithm, the number of floating point operations (FLOPs) is counted for processing 1 s of flight data. For this analysis, the IMU and GPS data are sampled at 100 Hz and 20 Hz, respectively. Therefore, a 5-to-1 prediction to measurement-update ratio is used in each KF. For instance, when no new GPS measurement is available, the predicted mean and covariance are carried to the next discrete time-step. The AVAE formulation is implemented at a 20-Hz update rate. The results for the computational load analysis are summarized in Table I. Table II shows that EKF is computationally more efficient than UKF within each of the presented GPS/INS formulations. However, the growth of computational load with respect to the dimension of the state vector appears to be steeper for EKF. Therefore, the computation requirement could be favoring the UKF if a sensor fusion algorithm requires a larger number of states.

B. Attitude Estimation Performance

In order to simplify the performance comparison among different sensor fusion algorithms, a performance index J is selected to reflect a composite estimation error including both the mean absolute error and error standard deviation for both roll and pitch angles with respect to the vertical gyro truth data

$$J = w_{\text{mean}}(|\phi_{\text{est}} - \phi_{\text{truth}}| + |\theta_{\text{est}} - \theta_{\text{truth}}|) + w_{\sigma}(\sigma[\phi_{\text{est}} - \phi_{\text{truth}}] + \sigma[\theta_{\text{est}} - \theta_{\text{truth}}]) \quad (40)$$

where the weights were chosen to be $w_{\sigma} = 0.3$, $w_{\text{mean}} = 0.2$, which places higher emphasis on the standard deviation of the estimation error. A smaller J indicates a better overall estimation performance of a sensor fusion algorithm.

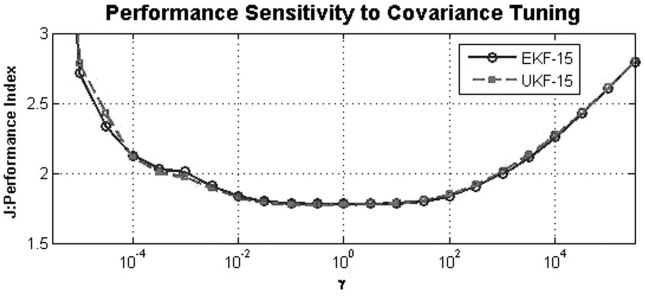

Fig. 5. Covariance tuning profile of 15-state EKF and UKF formulations.

TABLE I
Computational Performance of Attitude Estimation Algorithms

Formulation	Prediction	Update	# of FLOPS	Normalized FLOPS
AVAE	0	12480	12480	0.0665
EKF-3	180600	8600	189200	1
UKF-3	1319150	28620	1347770	7.12
EKF-9	189800	118980	308780	1.63
UKF-9	1888000	125760	2013760	10.64
EKF-15	713300	406180	1119480	5.92
UKF-15	3851800	375600	4227400	22.34

To ensure that performance comparisons were consistent for EKF and UKF, the same statistical assumptions were used (i.e., equivalent sensor error covariance matrices for both EKF and UKF) for sensor-level noise within the different filter implementations. In addition, a tuning test is performed to evaluate the sensitivity of UKF and EKF to statistical parameters. Specifically, the relative size difference between the process noise covariance matrix and measurement noise covariance matrix is adjusted with a scaling parameter γ,

$$Q = Q_0, \qquad R = \gamma R_0 \quad (41)$$

where a large γ represents an increase in the reliance of the prediction step while a small γ represents an increase in the reliance of the measurement-update procedure within the KF. As an example, Fig. 5 shows the estimation performance of the 15-state EKF and UKF as a function of γ, averaged over 23 flights. Fig. 5 shows that both EKF and UKF are well tuned when $\gamma = 1$ and they are similarly sensitive to covariance tuning. Additionally, both curves are relatively flat near their minimum point, indicating a large margin for tuning error during practical applications.

Table II summarizes the average performance over the 23 flights for each formulation in units of degrees. The 15-state UKF provides the best overall attitude estimation performance, both with respect to the mean and the standard deviation of

TABLE II
Attitude Estimation Performance Summary (All Units in Degrees)

Formulation	$\bar{J}$	$\sigma(J)$	$E(\lvert\phi_{\text{err}}\rvert)$	$\sigma(\phi_{\text{err}})$	$E(\lvert\theta_{\text{err}}\rvert)$	$\sigma(\theta_{\text{err}})$
AVAE	3.698	0.304	3.200	4.680	2.765	3.669
EKF-3	2.108	0.238	2.328	2.196	1.926	1.995
UKF-3	2.070	0.255	2.249	2.166	1.904	1.967
EKF-9	2.077	0.280	2.328	2.201	1.917	1.892
UKF-9	2.102	0.315	2.346	2.215	1.950	1.929
EKF-15	1.782	0.228	1.831	2.149	1.412	1.630
UKF-15	1.778	0.214	1.823	2.147	1.20	1.626

the performance index over all sets of flight data. This is closely followed by EKF-15, with nearly identical performance. Interestingly, the UKF-3 slightly outperforms the EKF-3, while the EKF-9 slightly outperforms the UKF-9. Also, as indicated in the 2nd column of Table II, the formulation that shows a higher performance also generally has less flight-to-flight performance variation.

To provide deeper insights into the difference between EKF and UKF in GPS/INS applications, a comparison of the linearization methods is conducted. As discussed in Section II-E, a fundamental difference between EKF and UKF is that EKF relies on an analytical linearization of the nonlinear state transition and observation equations, while UKF transforms random states statistically. As noted by Lefebvre, et al. [30] and Vercauteren and Wang [31] the sigma-point transformations can be viewed as a statistical linearization in the form of a weighted least squares regression (WLSR), where a linear transition matrix A and a bias term c are used to approximate the nonlinear function $f(\mathbf{x})$

$$f(\bar{\mathbf{x}}_{k-1|k-1}) = \bar{\mathbf{x}}_{k|k-1} \approx A\bar{\mathbf{x}}_{k-1|k-1} + c \tag{42}$$

which minimizes the weighted squared error between the true nonlinear predicted states and the model

$$e = f(\bar{\mathbf{x}}_{k-1|k-1}) - (A\bar{\mathbf{x}}_{k-1|k-1} + c) \tag{43}$$

where $\bar{\mathbf{x}}_{k-1|k-1}$ and $\bar{\mathbf{x}}_{k|k-1}$ are the weighted mean of sigma-points before and after being transformed through the nonlinear function, respectively. The solution for A and c that minimizes e is provided with a standard least square curve fitting method [31],

$$A = P_{\mathbf{x}_{k-1|k-1}\mathbf{x}_{k|k-1}}(P_{\mathbf{x}_{k|k-1}\mathbf{x}_{k|k-1}})^{-1} \tag{44}$$

and c is defined as

$$c = \bar{\mathbf{x}}_{k|k-1} - A\bar{\mathbf{x}}_{k-1|k-1}. \tag{45}$$

The difference between UKF and EKF for a specific application can be quantified by comparing results of the two linearization processes. To provide an example of this difference, Fig. 6 shows the matrix norms of the attitude submatrix within both EKF and UKF linearized time-update models (i.e., A), and the norm of their difference obtained over a single flight. Specifically, the top plot in Fig. 6 compares $\|A_k(\phi,\theta,\psi)\|_2$ obtained using both the EKF and UKF procedures, and $\|A_k^{\text{UKF}}(\phi,\theta,\psi) - A_k^{\text{EKF}}(\phi,\theta,\psi)\|_2$ is shown in the bottom plot. For this particular application, the linearization procedures produce nearly identical linear state transition matrixes for EKF and UKF, with the difference in the order of only a few hundredths of a degree. These differences have little effect on the overall estimation performance, as indicated in Table II.

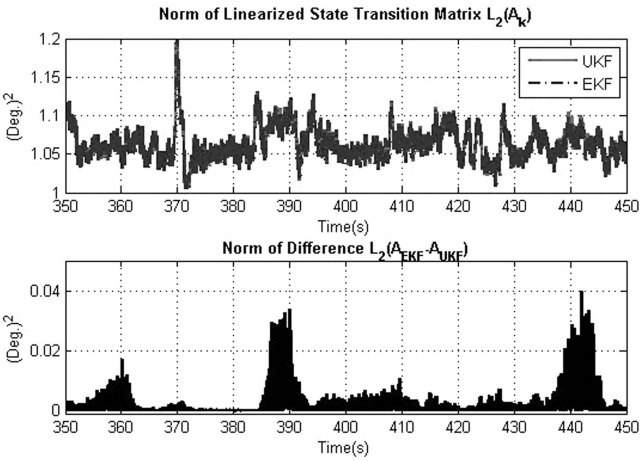

Fig. 6. EKF and UKF locally linearized attitude models over time.

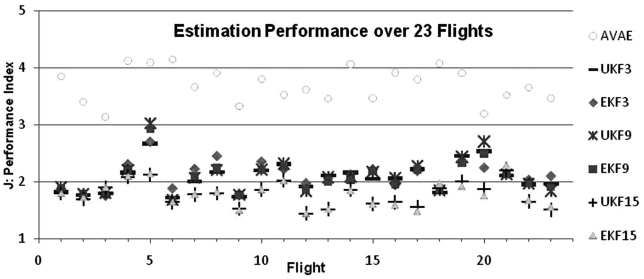

Fig. 7. Estimation performance index (J) of each sensor fusion formulations over 23 flights.

An overview of the estimation performance of all seven algorithms over 23 flights is presented in Fig. 7, which shows that the performance ranking for different formulations varies from flight-to-flight. This also highlights the importance of using a diverse set of flight data for the comparison study.

V. CONCLUSIONS

In small UAV-based applications the performance of sensor fusion algorithms often reflects a tradeoff between accuracy and the availability of on-board computational resources. Following a detailed comparative analysis, the AVAE has shown to be the most computationally efficient algorithm; therefore, it is considered to be more suitable for a low-cost real-time attitude reference system. Furthermore, the AVAE algorithm does not use a nonlinear estimator, which further eases implementation and tuning requirements. The EKF-3 offers a good balance between estimation performance and computational load. As shown in Table II, the EKF-3 ranks in the middle in terms of estimation performance, but is second only to AVAE in terms of computational requirements. While computationally expensive, the UKF-15 most closely matches the vertical gyroscope measurements. This formulation provides an excellent postprocessing solution.

This study utilized 23 diverse sets of flight data collected with four separate sensor systems with independent attitude truth measurement. A comparison analysis shows that EKF and UKF provide similar estimation performance throughout various GPS/INS attitude estimation formulations. In addition, within this application, EKF and UKF showed similar performance sensitivity with respect to process noise/measurement noise covariance tuning. Finally, with respect to the nonlinear state transition functions used for attitude estimation, the linearization methods employed by EKF and UKF were shown to produce very similar instantaneous linear models. Because the performance differences between EKF and UKF are minor, yet the computational requirements are very different, the EKF shows to be the most suitable nonlinear filtering solution for GPS/INS sensor fusion based attitude estimation. This claim is substantiated by the fact that the EKF-15 is significantly less computationally complex than even the UKF-3.

REFERENCES

[1] Changchun, L., et al.
The research on unmanned aerial vehicle remote sensing and its applications.
Proceedings of the IEEE 2010 International Conference on Advanced Computer Control (ICACC), Shenyang, China, 2010, pp. 644–647.

[2] Dascalu, S.
Remote sensing using autonomous UAVs suitable for less developed countries.
The International Archives of the Photogrammetry, Remote Sensing and Spatial Information Sciences, **34** (May 2006).

[3] Everaerts, J.
The use of unmanned aerial vehicles (UAVs) for remote sensing and mapping.
The International Archives of the Photogrammetry, Remote Sensing and Spatial Information Sciences, **XXXVI**, B1 (2008), 1187–1192.

[4] Jensen, A., Baumann, M., and Chen, Y.
Low-cost multispectral aerial imaging using autonomous runway-free small flying wing vehicles.
Proceedings of the IEEE International Geoscience and Remote Sensing Symposium (IGARSS), Boston, MA, 2008, pp. 506–509.

[5] Zhou, G. and Zang, D.
Civil UAV system for Earth observation.
Proceedings of the IEEE International Geoscience and Remote Sensing Symposium (IGARSS), Barcelona, Spain, 2007.

[6] Han, K. and DeSouza, G. N.
Instantaneous geo-location of multiple targets from monocular airborne video.
Proceedings of the 2009 IEEE International Geoscience and Remote Sensing Symposium (IGARSS), Cape Town, South Africa, July 2009, pp. IV 1003–1006.

[7] Suzuki, T., Amano, Y., and Hashizym, T.
Vision based localization of a small UAV for generating a large mosaic image.
Proceedings of 2010 SICE Annual Conference, Taipei, Oct. 2010, pp. 2960–2964.

[8] Nagai, M., et al.
UAV-borne 3-D mapping system by multisensor integration.
IEEE Transactions on Geoscience and Remote Sensing, **47**, 3 (Mar. 2009), 701–708.

[9] El-Diasty, M. and Pagiatakis, S.
A rigorous temperature-dependent stochastic modelling and testing for MEMS-based inertial sensor errors.
MDPI, **9** (2009), 8473–8489, ISSN 1324-8220.

[10] Kornfeld, R. P., Hansman, R. J., and Deyst, J. J.
Preliminary flight tests of pseudo-attitude using single antenna sensing.
Proceedings of the 17th Digital Avionics Systems Conference (AIAA/IEE/SAE), vol. 1, Bellevue, WA, 1998, pp. E56/1–E56/8, ISBN 0-7803-5086-3.

[11] Deyst, J. J., Kornfeld, R. P., and Hansman, R. J.
Single antenna GPS information based aircraft attitude redundancy.
Proceedings of the American Control Conference, vol. 5, San Diego, CA, 1999, pp. 3127–3131.

[12] Grewal, M. S., Weill, L. R., and Andrew, A. P.
Global Positioning, Inertial Navigation & Integration (2nd ed.).
Hoboken, NJ: Wiley, 2007.

[13] Kaplan, E. and Heagarty, C.
Understanding GPS Principles and Applications (2nd ed.).
Norwood, MA: Artech House, 2006.

[14] Kingston, D. B. and Beard, R. W.
Real-time attitude and position estimation for small UAVs using low-cost sensors.
AIAA 3rd Unmanned Unlimited Systems Conference and Workshop, Chicago, IL, Sept. 2004, AIAA-2004-6488.

[15] Crassidis, J.
Sigma-point filtering for integrated GPS and inertial navigation.
AIAA Guidance, Navigation and Control Conference and Exhibit, San Francisco, CA, 2005.

[16] Wendel, J., et al.
A performance comparison of tightly coupled GPS/INS navigation systems based on extended and sigma point Kalman filters.
Navigation: Journal of the Institute of Navigation, **53**, 1, (Spring 2006).

[17] van der Merwe, R., Wan, E., and Julier, S.
Sigma-point Kalman filters for nonlinear estimation and sensor fusion—Applications to integrated navigation.
AIAA Guidance, Navigation and Control Conference, Providence, RI, 2004, pp. 2004-5120.

[18] Gross, J., et al.
A comparison of extended Kalman filter, sigma-point Kalman filter, and particle filter in GPS/INS sensor fusion.
AIAA Guidance, Navigation and Control Conference and Exhibit, Toronto, Canada, 2010.

[19] Stengel, R. F.
Optimal Control and Estimation.
New York: Dover, 1994.

[20] Julier, S. and Uhlmann, J.
A new extension of the Kalman filtering to nonlinear systems.
Proceedings of SPIE, vol. 3069, 1997, pp. 50–62.

[21] St. Pierre, M. and Ing, D.
Comparison between the unscented Kalman filter and the extended Kalman filter for the position estimation module of an integrated navigation information system.
IEEE Intelligent Vehicles Symposium, Parma, Italy, 2004.

[22] Gu, Y., et al.
Autonomous formation flight: Hardware development.
IEEE Mediterranean Control Conference, Ancona, Italy, June 2006.

[23] Luczak, S., Oleksiuk, W., and Bodnicki, M.
Sensing tilt with MEMS accelerometers.
IEEE Sensors, **6**, 6 (Dec. 2006), 1669–1673.

[24] Crassidis, J. L., Markley, F. L., and Cheng, Y.
A survey of nonlinear attitude filtering methods.
AIAA Journal of Guidance, Control and Dynamics, **30**, 1 (Jan.–Feb. 2007), 12–28.

[25] Singla, P., Mortari, D., and Junkins, J.
How to avoid singularity for Euler angle set?
AAS 2004 Space Flight Mechanics Meeting Conference, Maui, HI, Feb. 9–13, 2004, AAS 04-190.

[26] Stevens, B. L. and Lewis, F. L.
Aircraft Control and Simulation (2nd ed.).
Hoboken, NJ: Wiley, 2003.

[27] Roskam, J.
Airplane Flight Dynamics and Automatic Flight Controls.
DARcorporation, Lawrence, KS, 2003.

[28] El-Diasty, M. and Pagiatakis, S.
Calibration and stochastic modeling of inertial navigation sensor errors.
Journal of Global Positioning Systems, **7**, 2 (2008), 170–182.

[29] Crassidis, J. and Junkins, J.
Optimal Estimation of Dynamic Systems.
New York: Chapman & Hall/CRC, 2004.

[30] Lefebvre, T., Bruyninckx, H., and De Schuller, J.
Comment on "A new method for the nonlinear transformation of means and covariances in filters and estimators."
IEEE Transactions on Automatic Control, **47**, 8 (2002), 1406–1409.

[31] Vercauteren, T. and Wang, X.
Decentralized sigma-point information filters for target tracking in collaborative sensor networks.
IEEE Transactions on Signal Processing, **53**, 8 (Aug. 2005).

[32] Simon, D.
Optimal State Estimation.
Hoboken, NJ: Wiley, 2006.

[33] Gu, Y., et al.
Autonomous formation flight—design and experiments.
In *Aerial Vehicles*, I-Tech Education and Publishing, Austria, Jan. 2009, ch. 12, pp. 233–256, ISBN 978-953-7619-41-1.

[34] Gu, Y.
Design and flight testing actuator failure accommodation controllers on WVU YF-22 research UAVs.
Ph.D. dissertation, Dept. of Mechanical and Aerospace Engineering, West Virginia University, 2004.

[35] Gross, et al.
Advanced research integrated avionics (ARIA) system for fault-tolerant flight research.
AIAA Guidance, Navigation and Control Conference and Exhibit, Chicago, 2009.

[36] Wan, E. and van der Merwe, R.
The unscented Kalman filter for nonlinear estimation.
Proceedings of IEEE 2000 AS-SPCC Symposium, Lake Louise, Alberta, CA, 2000.

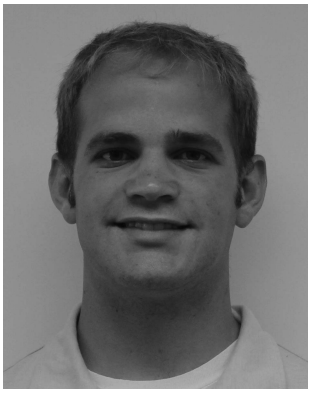

Jason N. Gross (S'11) was born in Charleston WV in 1985. In 2007, he received his Bachelor of Science in mechanical engineering and a Bachelor of Science in aerospace engineering. from West Virginia University, Morgantown, WV.

Since 2008, he has been a graduate research assistant at West Virginia University working towards a Ph.D. in aerospace engineering, and since 2009 he has been a NASA WV Space Grant Consortium graduate research fellow. He interned at NASA Goddard Space Flight Center in the summers of 2005 and 2007.

Mr. Gross is a student member of AIAA.

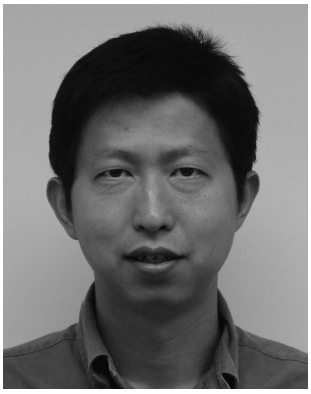

Yu Gu (M'04) was born in Huainan, China in 1975. He received a B.S. degree in automatic controls from Shanghai University in 1996, an M.S. degree in control engineering from Shanghai Jiaotong University in 1999, and a Ph.D. degree in aerospace engineering from West Virginia University, Morgantown, in 2004.

Since 2005 he has been a research assistant professor in the Department of Mechanical and Aerospace Engineering at West Virginia University. His main research interests include sensor fusion, flight control, and small unmanned aerial vehicle (SUAV) design, instrumentation, and flight testing.

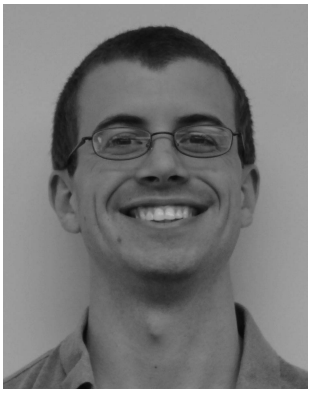

Matthew B. Rhudy received a Bachelor of Science in mechanical engineering in 2008 from The Pennsylvania State University, State College, PA, and a Master of Science in mechanical engineering in 2009 from the University of Pittsburgh, Pittsburgh, PA.

Since 2010, he has been working towards a Ph.D. in aerospace engineering as a graduate research assistant at West Virginia University, Morgantown, WV. He worked as a graduate student researcher at the University of Pittsburgh from 2008 to 2009, an undergraduate teaching intern at The Pennsylvania State University from 2007 to 2008, and a quality engineering intern in the summer of 2007 for Tyco Electronics.

Mr. Rhudy is currently a student member of AIAA.

Srikanth Gururajan received his Ph.D. degree in aerospace engineering from West Virginia University, Morgantown, in 2006.

He is currently working as a post-doctoral fellow in the Department of Mechanical and Aerospace Engineering at West Virginia University.

Dr. Gururajan is a senior member of the AIAA.

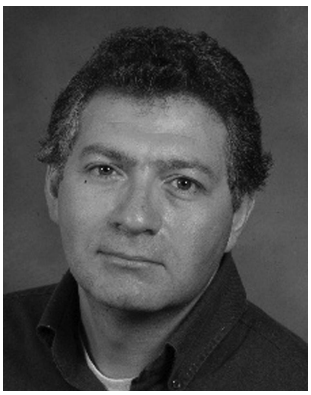

Marcello R. Napolitano was born in Pomigliano d'Arco, Italy, in 1961. He holds a Master degree in aeronautical engineering from the 'Universita' di Napoli–Federico II', Naples, Italy, in 1985 and a Ph.D. in aerospace engineering from Oklahoma State University, Stillwater, OK, in 1989.

He is currently a professor in the Department of Mechanical and Aerospace Engineering (MAE), West Virginia University. He is also the Director of the Flight Control System Research Laboratory in the MAE Department at WVU.

Dr. Napolitano is the author or coauthor of more than 130 technical publications in the general area of fault tolerant flight control systems and UAV-related research. Additionally, he is the author of the textbook, *Aircraft Dynamics: From Modeling to Simulation* (Wiley, 2011). He is a member of the AIAA.